# Removal of RB5 Dye Using a Mexican Natural Zeolite: Characterization and Evaluation

José Domenzain-Gonzalez, José J. Castro-Arellano* and Luis A. Galicia-Luna
Laboratorio de Termodinámica, S.E.P.I.-E.S.I.Q.I.E. Instituto Politécnico Nacional, UPALM, Edif. Z, Secc. 6, 1ER piso, Lindavista C.P. 07738, México D. F., México.

**Abstract**— In this work Mexican Natural Zeolite (MNZ) from Tehuacán, Puebla, México was used. This material is an attractive mineral due to their physicochemical properties and its contents of semiconductor materials such as Fe, Ti and Zn, which can be employed in degradation processes. The raw mineral was subjected to a milling process and calcination at different temperatures (200 °C to 700 °C), in order to observe effect of this variable in the composition, morphology, structural and textural properties of mineral. Atomic Absorption (AA), X-ray diffraction (XRD), EDS, Adsorption – Desorption of $N_2$, Micro Raman Spectroscopy and Diffuse Reflectance techniques were employed to determine its physicochemical properties. Then, zeolite material was used as a porous powder catalyst for Reactive Black 5 (RB5) dye degradation. Catalytic evaluation of MNZ was carried out in a batch reactor using an UV-LED lamp (0.3 W and 405 nm). For all measurements, 2 g/L of $H_2O_2$ as oxidizing agent was added with initial RB5 dye concentration of 100 ppm at pH 3.5. Tests were conducted at 25 °C and at calcination temperature of 700 °C. The whole experiments were done at atmospheric pressure (0.78 bar) and at zeolite concentrations of 0.072, 0.100, 0.170, 0.510 and 1.000 g/L. Dye removal treatment was performed with and without ultraviolet irradiation. Reactions monitoring were carried out using UV-vis spectroscopy at wavelength of 597 nm, corresponding to chromophore of dye molecule. Also, were used Total Organic Carbon (TOC) and Inorganic Carbon (IC) analysis, obtaining a decolouration between 80 % and 85 % and the maximum removal of RB5 dye of 50 % was achieved.

**Index Terms**— Atomic Absorption, Brunauer-Emmett-Teller method (BET), characterization, clinoptilolite, decoloration, Diffuse Reflectance, Mexican natural zeolite (MNZ), reactive black 5 (RB5), Scanning Electron Microscope (SEM), X-ray diffraction (XRD).



## 1 Introduction

In the world there are a large amount of deposits of natural zeolite (NZ), distributed in various areas. In Mexico, major part of resources for zeolites are located in states of Sonora, Oaxaca, Puebla, San Luis Potosi, Guanajuato, Michoacán, Guerrero and Tamaulipas [1].

Natural zeolites belong to family of crystalline hydrated aluminium silicate of volcanic origin [2], its porous structure is regular and homogeneous mainly formed with tetrahedral silicates $(SiO_4)^{4-}$, joined together through oxygen atoms with $Al^{3+}$. Since, Al has a positive charge less than Si, so the network is left with a negative charge [3], and it is compensated by a cation such as $Na^+$, $K^+$, $Ca^{2+}$, $Fe^{2+}$ or $Mg^{2+}$. The cation exchange depends on nature of zeolite. Minerals with a low Si/Al ratio have a higher ion exchange capacity [4]. In nature, there are various types of zeolites, being clinoptilolite, mordenite, erionite and ferrite the most abundant and accessible [5]. These materials have shown different commercial applications such as ammonia and ammonium adsorption [6], drying and removal of $CO_2$ from gases, removal of compounds with S, Hg, NOx and SOx and also for separation of compounds such as xylene, olefins, oxygen in air and in refining sugar [7].

In addition, natural zeolites have been used as raw material to synthesize other zeolites such as "Y" [8, 9].

Zeolites have a beneficial impact on treatment of effluents contaminated with organic matter [10], either as an adsorbent [11] or as catalyst support [12]. One of the most common problems with effluent contamination is due to synthetic dyes from textiles, paper fabrication and other processes. Dyeing in textile industry is the most aggressive process to environment because of large quantities of wastewater production with dye, textile auxiliaries and various chemicals used [13]. According to importance of this industry, different types of dyes have been developed based in the chromophore structure. On the other hand, azo dyes, characterized by having an azo group, which comprises two nitrogen atoms (-N = N-), are the most used type of dyes in this industry [14].

Decolouration in the washing process is about 15% of the total pollution of the textile industry [15].

Furthermore, presence of dyes in natural water source is directly associated with toxicity and carcinogenic property caused by compounds such as surfactants, suspended solids, organochloric compounds, etc. For this, removal of dyes in wastewater from the textile industry has taken more attention in research and industry [16]. Since, most of dyes used are resistant to natural oxidation processes, different techniques, such as activated carbon adsorption [17, 18], filtration [19] and biodegradation [20], have been used for the removal of organic pollutants of wastewater. However as is known, physical methods only transfer pollutants from one phase to another. In contrast, biological treatments are not always successful since some dyes exhibit biological resistance [21].

Moreover, advanced oxidation processes (AOP) are methods

- *José Domenzain-Gonzalez, Laboratorio de Termodinámica, S.E.P.I.-E.S.I.Q.I.E. Instituto Politécnico Nacional. josedomenzain88@gmail.com.*
- **Corresponding Autor: José J. Castro-Arellano, Laboratorio de Termodinámica, S.E.P.I.-E.S.I.Q.I.E. Instituto Politécnico Nacional. jjcastro@ipn,mx.*
- *Co-Author: Luis A. Galicia-Luna, Laboratorio de Termodinámica, S.E.P.I.-E.S.I.Q.I.E. Instituto Politécnico Nacional.*

based on physicochemical processes which can produce huge changes in the structure of contaminant, due to their poor selectivity and oxidizes most organic compounds and high production of hydroxyl radicals (•OH), which are highly reactive and attack most organic molecules, which make these processes more efficient than mass transfer methods.

Meanwhile, contaminants are dumped as wastes into liquid effluents, which become more difficult to remove by conventional treatment processes. It is necessary to develop or improve these processes by obtaining economical materials to accelerate transformation of pollutants to non-toxic products or to eventual mineralization.

There are several works where Ti and Fe are used with synthetic zeolites as photocatalytic materials, however, there are a lack reports with natural zeolites, which have a large potential as catalyst in different applications due to, in their composition that have metals as Fe and Ti. Whereby, it is important to determine the characteristics of these minerals for possible use in photocatalysis and heterogeneous catalysis [22].

The aim of this study was to observe the effect of calcination temperature on properties of Mexican natural zeolites (MNZ) from Tehuacán, Puebla, México and its subsequent use at different concentrations as a catalyst in removal of RB5 dye. This ore was characterized to determine their overall composition, zeolitic phases present, and presence of semiconductor materials in ore to use as a promoter in removal of Reactive Black 5 dye, under and without ultraviolet (UV) radiation.

## 2. Materials and methods

In this work was used a MNZ constituted mainly of clinoptilolite type. Evaluation of this ore as a catalyst was performed using RB5 dye with a stated purity of 55 % provided from Sigma-Aldrich. Fermont supplied hydrogen peroxide with purity 50 % (used as oxidizing agent) and hydrochloric acid (used to fix the pH of the solution). For preparation of aqueous solution, distilled water was used. The mass of all compounds were determined using a comparator balance (Sartorius LC1201S) with standard uncertainty of $1\times10^{-7}$ kg.

### 2.1. MNZ clinoptilolite conditioning

The MNZ was subjected to a mechanical milling process by 180 min using a ball mill (with capacity of 1 kg) and with three different ball sizes: 2.57, 2.05 and 1.25 cm of diameter, obtaining different particle size. This particle size distribution was obtained using a mechanical sieving equipment (Ro-Tab RX-29) with meshes of No. 70 to No. 400, corresponding to interval from 212 to 38 μm. Scanning Electron Microscopy was used to identify particles between 0.5 to 75 μm. Then, cone and quartering technique was used and different samples were taken, which were calcinated at different temperatures in a muffle (Vulcan model 3-130), increasing temperature with a rate of 2 °C per min and by steps of 100 °C, where each step was kept for 60 min.

After the desired calcination temperature was reached, MNZ was kept at these conditions for 180 min in air atmosphere.

### 2.2. Sample characterization

Elemental analysis of MNZ was determined by Atomic Absorption (AA equipment Perkin Elmer, AAnalyst 200), in which the overall composition expressed as metal oxide percent mass. Moreover, microstructure of material was observed in a Scanning Electron Microscope (SEM JEOL, JSM 7800F) with EDS detector and resolution from (0.8 to 1.2) nm and (15 to 1) kV, respectively. The composition of crystal was evaluated in different points on surface of one sample (four times for each temperature).

Structural analysis was determined using X-ray diffraction (XRD) equipment (Siemens, D500) with copper anode and nickel filter. This instrument was used at 35 KV and 25 mA with a scanning velocity of 2 degrees per min. Raman spectra were gotten with equipment (Olimpus, BX41-HR800) at wavelength of 785 nm for excitation and Diffuse Reflectance was determined using UV-Vis-NIR spectrophotometer (Agilent, Cary 5000). On the other hand, deconvoluted diffuse reflectance absorption spectra were determined using Origin 2016 software.

Finally, adsorption and desorption of nitrogen measurements in uncalcined and calcined materials were done at different temperatures. Surface area was determined by Brunauer-Emmett-Teller method (BET) [23] (Quantachrome, NovaWin) at temperature of liquid nitrogen (-196.15 °C). The calcined samples (550 °C and 700 °C) were degassed under vacuum at 200 °C for 4 h before measurement. While uncalcined zeolite sample (25 °C) was degassed under vacuum at 120 °C for 5 h to avoid changes in surface area and pore size by effect of temperature. Micropore volume was determined by graphical method [24], whereas differential distribution of pore volume was evaluated by Density Functional Theory (DFT) method [25]. One section of adsorption isotherm was taken to determine the pore size distribution to evade interference from consequences of interconnectivity related with tensile strength effects (TSE), which happen around the nearest point below hysteresis loop of desorption isotherm [26].

### 2.3. Catalytic tests

The catalytic activity evaluation of MNZ in removal of RB5 dye was carried out in a batch reactor with volume of 150 mL, RB5 dye solution was continuously stirred and UV LEDs lamp was used which designed for this system, which emitted a signal at 405 nm with a power of 0.3 W was placed in a coating used quartz, and placed in the centre of reactor. The pH of experiments was maintained in the range of 3.5 to 3.7 using HCl to adjust this variable. In addition, hydrogen peroxide at 50% was used as a source of hydroxyl radicals.

Finally, the reaction progress was monitored using UV-vis spectrophotometer (Ocean Optics, Jaz) with a radiation source (Analytical Instrument Systems Inc., DT 1000 CE) and optical fibers (Ocean Optics, QP300-1- SR) at the maximum absorbance of RB5 (597 nm). Total Organic Carbon (TOC) for removal reactions of RB5 dye was analysed using TOC Analyser (EG InnovOx, Sievers). To perform calibration of instrument, sucrose and sodium carbonate were used to determine TOC and Inorganic Carbon (IC), respectively.

## 3. Results and Discussion

### 3.1. Atomic Absorption (AA)

The compositions of uncalcined (25 °C) and calcined MNZ (550 °C and 700 °C), were determined by AA (Table 1). With the aim to observe the effect of calcination temperature in overall composition of zeolite, the results were expressed in percentage weight of metal oxides. The material was mostly composed of silicon and aluminum, and to a lesser extent of other metals such as iron. A characteristic parameter of zeolites was Si/Al ratio, which explains nature of material. Si/Al ratio for MNZ samples at 25, 550 and 700 °C were 4.648, 4.395 and 4.641, respectively, indicating that it has a phase of clinoptilolite type. Since values of this zeolite was ranging from 4.250 to 5.250 [4], it is representing an acidity in material, besides presence of ions (Fe, Na, K, Ca, Mg, Ti and Zn) were observed which are representative of the mineral. It was also observed that calcination temperatures did not change the overall composition of mineral but variations of values were obtained due to lack of homogeneity owing the nature of mineral.

TABLE 1. COMPOSITION OF NATURAL ZEOLITE AT 25, 550 AND 700 °C.

| Oxide | Calcination temperature | | |
|---|---|---|---|
| | 25 °C | 550 °C | 700 °C |
| $SiO_2$ | 57.830 | 57.191 | 55.644 |
| $Al_2O_3$ | 12.440 | 13.010 | 11.989 |
| $Fe_2O_3$ | 2.570 | 2.590 | 2.696 |
| CaO | 13.970 | 14.145 | 15.494 |
| MgO | 10.340 | 10.097 | 11.265 |
| $TiO_2$ | 0.101 | 0.116 | 0.111 |
| $Na_2O$ | 0.782 | 0.759 | 0.684 |
| $K_2O$ | 1.919 | 2.055 | 2.088 |
| $Li_2O$ | 0.020 | 0.019 | 0.018 |
| ZnO | 0.010 | 0.011 | 0.010 |
| Si/Al | 4.648 | 4.395 | 4.641 |

*Composition of Mexican Natural Zeolite in percentage weight of metal oxide.*

### 3.2. Scanning Electron Microscopy (SEM)

Micrographs of MNZ crystals at different calcination conditions in range of 200 °C to 700 °C are shown in Figure 1. In this Figure were observed particles of irregular shape in the particle size range from 0.5 to 75 µm. However, as be mentioned before, by mechanical sieving a maximum particle size of 212 µm was determined. At temperatures up to 700 °C, the crystallinity of the material is preserved.

EDS spectra (Figure 2) of MNZ, showed presence of Si and Al and small amounts of Ca, Mg, Na, K and Fe. EDS spectra corresponding to calcinated sample at 400 °C, 700 °C and uncalcined indicated that spectrum intensity decreases as temperature increasing. In order to variety the Si/Al ratio the elemental analysis was conducted in different zones of a calcined mineral sample at 600 °C and 700 °C, elemental analysis expressed in percentage weight and is shows in Table 2.

At 600 °C, four distinct crystals zones composition was obtained and Si/Al ratio of two zones were 4.642 to 4.996, corresponding to clinoptilolite, which is in good agreement to XRD analysis. Potassium (K) was found in greater proportion compared to other elements. The results show (Table 2) that the crystals are considered like zeolite clinoptilolite-K type. By other side, Mg was not observed in the samples at 600 °C.

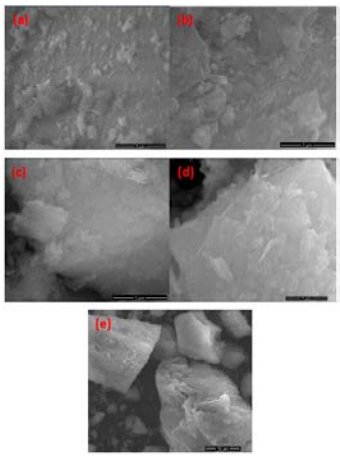


Fig. 1. Micrographs of MNZ: a) uncalcined; calcined at: b) 200 °C, c) 400 °C, d) 600 °C and e) 700 °C.

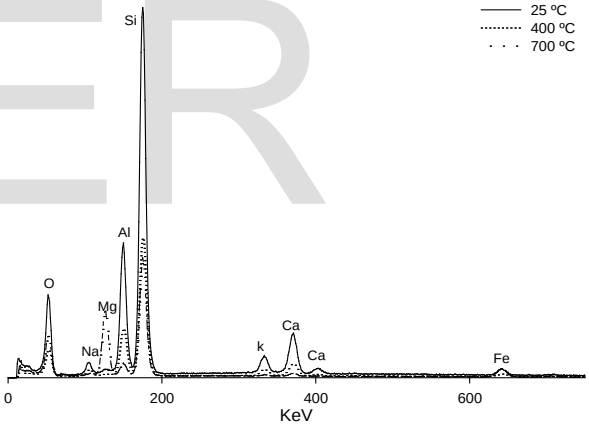


Fig. 2. EDS of MNZ at 25, 400 and 700 °C.

On the other hand, calcined sample at 700 °C shows great variations in composition, a sample with Si/Al ratio of 3.046 which corresponds to erionite phase (Si/Al = 3 - 3.6 [27]), and in another zone with a 10.250 ratio, corresponding to mordenite (Si/Al = 5.5-10 [28]) all samples have a high content of Fe and Mg, while other two zones were identified as clinoptilolite-K having a Si/Al ratio of 4.599 and 5.325, respectively. From this elemental analysis, heterogeneity of the mineral composition was confirmed.

In Table 3, average of EDS to zeolite at different calcination temperatures were shown at 25 °C and 400 °C have a Si/Al ratio of 3.469 and 3.546 which are attributed to erionite phase. Whereas at 200 °C, 600 °C and 700 °C, the major phase was clinoptilolite-K, while at 800 °C phase was mordenite accord-

ing to its Si/Al ratio = 5.537. From this micro analysis it was observed the heterogeneity that composition varies according to each examined zone samples and heat treatment.

TABLE 2. ELEMENTAL ANALYSIS OF A SAMPLE OF MNZ IN VARIOUS CRYSTALS AT 600 °C AND 700 °C.

| Element | *600 °C* | | | | *700 °C* | | | |
|---|---|---|---|---|---|---|---|---|
| OK | 42.750 | 36.950 | 42.120 | 43.060 | 30.140 | 33.490 | 40.330 | 38.530 |
| NaK | 2.130 | 1.650 | 1.650 | 1.830 | 3.240 | 0.610 | 1.650 | 2.070 |
| MgK | - | - | - | - | 0.530 | 18.590 | 0.440 | - |
| AlK | 8.980 | 9.510 | 8.610 | 8.770 | 13.980 | 3.550 | 9.190 | 8.530 |
| SiK | 41.690 | 44.920 | 43.020 | 42.240 | 42.590 | 36.400 | 42.270 | 45.430 |
| KK | 2.640 | 4.810 | 2.500 | 1.860 | 2.060 | 0.410 | 4.270 | 3.040 |
| CaK | 0.790 | 0.990 | 1.270 | 1.080 | 5.980 | 0.950 | 1.210 | 1.400 |
| FeK | 1.020 | 1.170 | 0.820 | 1.160 | 1.480 | 6.010 | 0.650 | 1.000 |
| Si/Al | 4.642 | 4.723 | 4.996 | 4.816 | 3.046 | 10.253 | 4.599 | 5.325 |

TABLE 3. AVERAGE EDS ANALYSIS OF MNZ CALCINED SAMPLES AT 25, 200, 400, 600, 700 AND 800 °

| Element | 25 °C | 200 °C | 400 °C | 600 °C | 700 °C | 800 °C |
|---|---|---|---|---|---|---|
| O K | 32.790 | 31.450 | 32.600 | 38.390 | 35.622 | 31.480 |
| NaK | 1.830 | 0.690 | 2.830 | 2.842 | 1.892 | 2.120 |
| MgK | 0.430 | 0.440 | 0.440 | 0.420 | 4.89 | 0.380 |
| AlK | 12.070 | 9.810 | 12.230 | 8.967 | 8.812 | 9.210 |
| SiK | 41.880 | 51.770 | 43.370 | 42.967 | 41.672 | 51.00 |
| K K | 2.610 | 2.470 | 2.380 | 2.320 | 2.445 | 2.980 |
| CaK | 6.180 | 1.860 | 4.430 | 2.292 | 2.385 | 1.410 |
| FeK | 2.210 | 1.510 | 1.710 | 1.025 | 2.285 | 1.430 |
| Si/Al | 3.469 | 5.277 | 3.546 | 4.791 | 4.729 | 5.537 |

### 3.3. X-Ray Diffraction (XRD)

XRD patterns for uncalcined (25 °C) and calcinated zeolites (between 500 °C and 700 °C) are shown in Figure 3. Signals of these samples were clustered peaks at 2θ values between 20° and 40°, where they were identified as mixture of zeolites, the major phase was identified as clinoptilolite - heulandite and second one as erionite – mordenite. Sample also had impurities such as feldspar and quartz at 25 °C.

It was also observed that signal intensities changed due to increase calcination temperature below 25°, the species present almost disappeared, except for erionite. Concerning the heulandite phase was observed that up to 500 °C persists in sample, above this temperature the heulandite collapses [29, 30]. Moreover, the strongest signals, localized between 27° to 40°, when temperature increases, these signals decreased, which corresponding to clinoptilolite, erionite, mordenite and quartz. Base of the peaks were wide, which indicated a loss of zeolitic species present and also the material crystallinity decreased at high temperature. According to international literature, the erionite begins to disappear at 840 °C [31]. The clinoptilolite persists up to 900 °C [32] like mordenite [33], this indicates that overall composition does not change, even with the collapse of heulandite phase as well as it was determined by atomic absorption analysis.

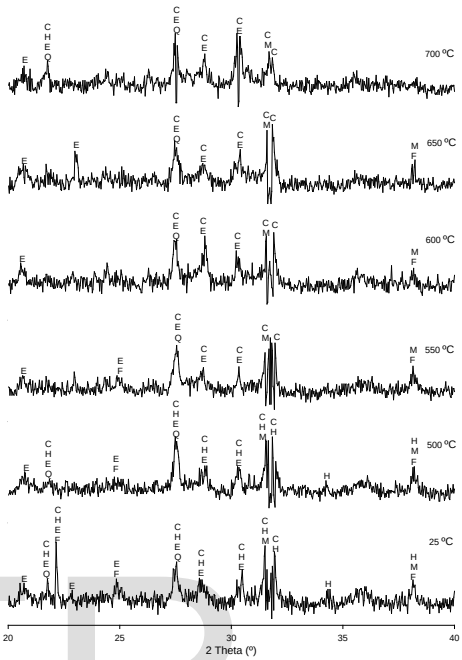


Fig. 3. XRD patterns of uncalcined (25 °C) and calcined zeolite at 500, 550, 600, 650 and 700 °C.
C: Clinoptilolite; H: Heulandite; E: Erionite; M: Mordenite; F: Feldspar y Q: Quartz.

### 3.4. Micro Raman Spectroscopy

The Figure 4 shows images and their corresponding Raman spectra of uncalcined (Figure 4a) and calcined MNZ at 550 °C (Figure 4b), which were determined. In image of Figure 4a was observed large amount of white areas and only one brown cluster particle, in contrast, image Figure 4b we was detected more amount of orange areas, which represents an incrementing of quantity of colored particles. Micro-Raman spectra of these particles in both Figures correspond to characteristic Raman vibrational modes with rutile phase in accordance to X. Liu, et al. [34] (143, 245, 442, 449, 609, 612 $cm^{-1}$).

On the other hand, the Figure 5 shows optical images and Raman spectra of calcined samples at 600 °C with brown and orange particles and crystalline particles, and calcined samples at 650 °C where was observed only one orange cluster in a large white area, respectively. At 600 °C and 650 °C of calcination temperatures, MNZ presented an intense signal in 143 $cm^{-1}$, which corresponds to rutile (Figure 5a and 5b). The other signals of Raman spectra for both samples corresponding to vibrational modes in 222, 292, 404, 495 and 607 $cm^{-1}$, which are characteristics of crystalline structure of ferric oxide ($\alpha$-$Fe_2O_3$), it is known as hematite (Figure 5a and 5b) [35, 36]. This indicate that the study area correspond to crystalline phase of $TiO_2$ with small amounts of iron oxide.

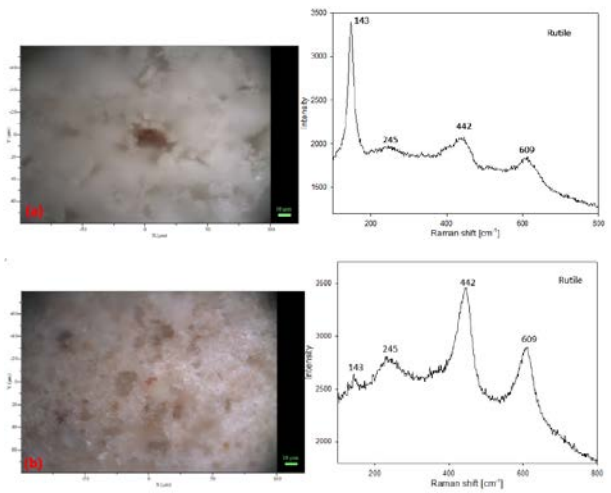


Fig. 4. Optical images and their corresponding micro-Raman spectra of MNZ: a) uncalcined and b) calcined at 550 °C.

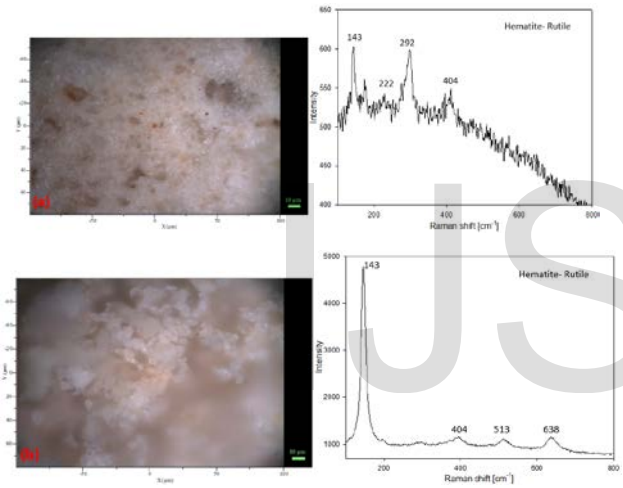


Fig. 5. Optical images and their corresponding micro-Raman spectra of calcined MNZ: a) at 600 °C and b) at 650 °C.

In Figure 6a, it was observed the presence of hematite which is as red cluster to according Raman spectra, moreover, rutile and clinoptilolite-K (Figure 6b) was verified, according to vibrational modes clinoptilolite at 270 and 410 $cm^{-1}$ [37]. Finally, Raman spectrum analysis of black particles showed signals at 193, 219, 346, 630 and 668 $cm^{-1}$ (Figure 6c), which indicated the presence of magnetite [38, 39] in combination with hematite. It explains that semiconducting materials as hematite persist in MNZ with increasing calcination temperature.

### 3.5. UV-Visible Diffuse Reflectance Spectroscopy (UV-vis-DR)

The Kubelka-Munk model F(R) versus wavelength of MNZ at different calcination temperatures (500, 550, 600, 650, 700 °C) and uncalcined (25 °C) are presented in Figure 7. It was noticed that the intensity of samples at 500, 550, 600 and 700 °C, increase as temperature increased. However, samples at 25 °C and 650 °C not exhibited the same behavior, this is mainly due to mineral composition. Band position can be used for estimate Fe species present in ore as nucleality from FexOy moieties, present on zeolite surface.

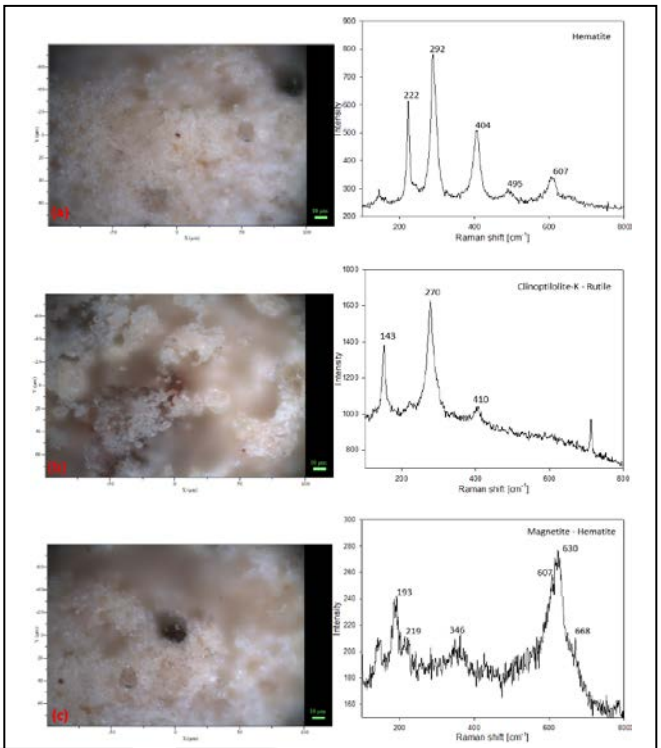


Fig. 6. Optical images and their corresponding micro-Raman spectra of calcined MNZ sample at 700 °C.

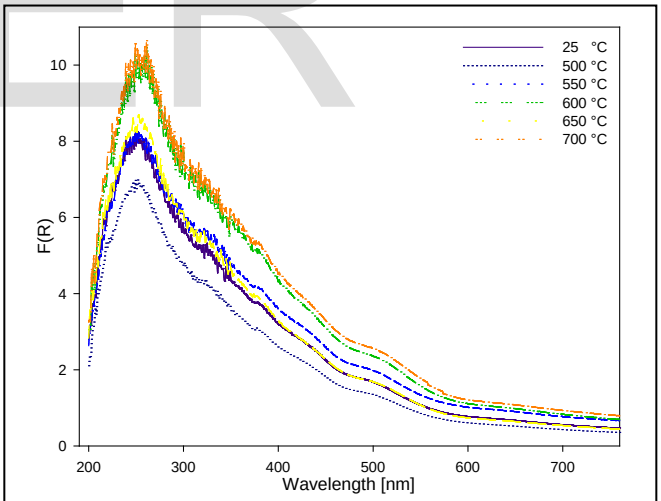


Fig. 7. UV-vis diffuse reflectance spectra of uncalcined MNZ (25 °C) and calcined MNZ at 500, 550, 600, 650 and 700 °C.

Spectral deconvolution of an UV-vis spectra was performed using the smallest number of Gaussian sub-bands as are shown in Figure 8, for MNZ sample calcined at 500 °C. Spectra were characterized through a major band (252 nm), related to charge transfer of iron from isolated ions of $Fe^{3+}$ in tetrahedral coordination [40], intensity of this band was linked with Fe content. This means that signals can be taken as fingerprint of highly dispersed Fe ions of both inside and outside of the network and the band became more intense when increasing Fe [41].

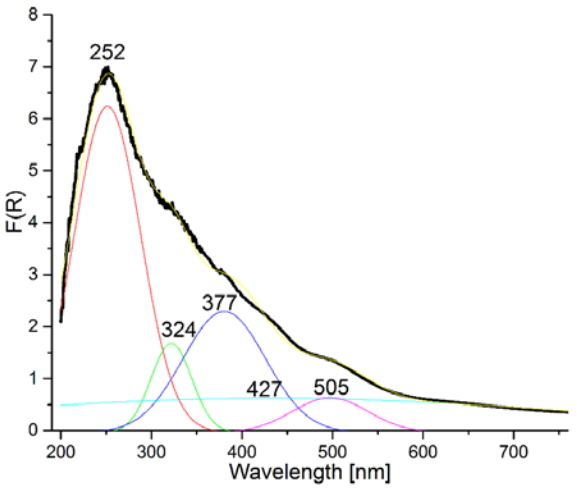


Fig. 8. Deconvoluted UV-Vis diffuse reflectance absorption spectra of MNZ sample calcined at 500 °C.

Bands between 300 - 400 nm were assigned to octahedral $Fe^{3+}$ in small groups of FexOy [42], while more extensive were Fe groups, then band was shifted towards visible region (427 nm) due to particles of $Fe_2O_3$ present in network [43]. Also, at 505 nm can be identified a d – d transition, which represent $Fe^{3+}$ ion in tetrahedral symmetry [41, 42].

### 3.6. Superficial Textural Characterization by $N_2$ Isotherms

Using adsorption - desorption of nitrogen, the surface area, pore volume and pore diameter of MNZ samples were determined. Adsorption - desorption curves are type IV with H3 hysteresis loop (Figure 9). Since, multilayers physisorption isotherms are associated with capillary condensation in mesoporous materials, which inferred that the pores were groove shaped [44].

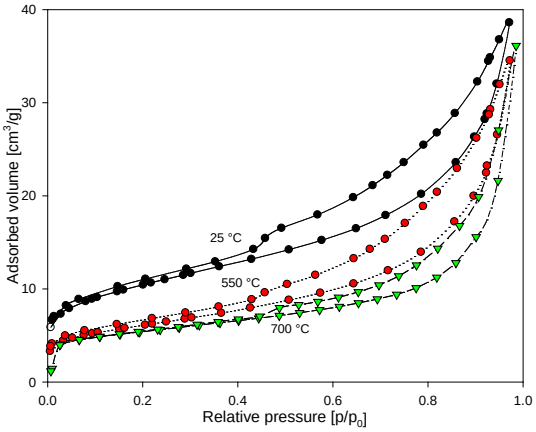


Fig. 9. Adsorption-desorption isotherm of nitrogen in MNZ at ● 25 °C, ● 550 °C and ▼ 700 °C.

Due to irregularity of pores, adsorption and desorption showed hysteresis loop, a characteristic of mesoporous material. By using DFT method, it was observed that the highest accumulation of pore size was between 2 - 10 nm, within range of up to 25 nm (Figure 10).

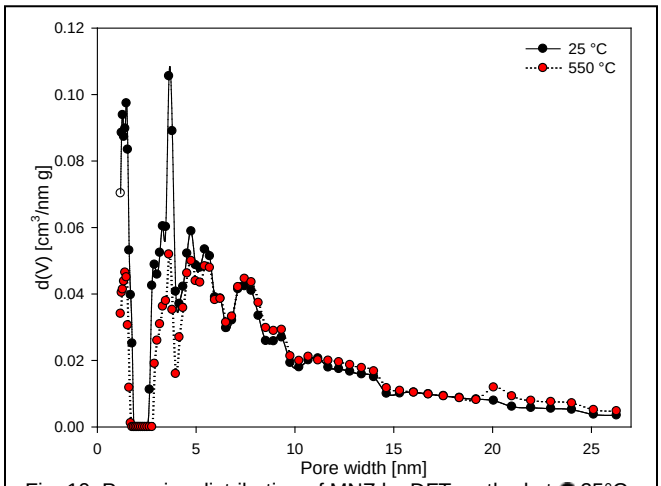


Fig. 10. Pore size distribution of MNZ by DFT method at ● 25°C and ● 550°C.

In Table 4, surface area, pore volume and pore diameter of MNZ samples are shown. It was observed that with increasing temperature, surface area decreased from 36 $m^2/g$ at uncalcined to 16 $m^2/g$ at 700 °C, pore volume was decreased while pore diameter was increased with calcination [45]. This effect was due to gradual loss of zeolite crystalline phase with temperature increase.

### 3.7. Catalytic evaluation of MNZ

The removal test of RB5 dye was carried out at 100 ppm, the solution was kept under constant stirring and HCl was added to adjust pH to 3.5. In addition, 2 g/L of $H_2O_2$ as oxidizing agent was added, whereas, MNZ as catalyst was aggregated in

TABLE 4. SURFACE AREA, PORE VOLUME AND PORE DIAMETER OF MNZ AT 25, 550 AND 700 °C.

| Calcination temperature [°C] | Surface area [$m^2/g$] | Pore volume [$cm^3/g$] | Pore diameter [nm] |
|---|---|---|---|
| 25 | 36.177 | 0.597 | 6.600 |
| 550 | 21.321 | 0.534 | 10.000 |
| 700 | 16.165 | 0.421 | 10.440 |

different concentrations of 0.072, 0.100, 0.170, 0.510 and 1.0 g/L. In these experiments were used uncalcined MNZ (25 °C) and MNZ calcined at different temperatures (from 500 °C to 700 °C). Reactions were monitored for 180 minutes in intervals of 10 minutes, using an UV-vis spectrometer. The measurements were performed at 597 nm which corresponded to chromophore of RB5 dye molecule, which gives colouration.

In this paper, only results with MNZ uncalcined at 25 °C and MNZ calcined at 700 °C are shown, both with and without UV radiation, because the MNZ calcined at 700 °C had higher activity than zeolites calcined at lower temperatures.

When uncalcined MNZ and without UV radiation was used, the results show no catalytic activity in any of the five cases (concentrations of 0.072, 0.100, 0.170, 0.510 and 1.0 g/L). In Figure 11a, it can be seen that the slope of the curve (dye concentration against time) is a constant, which means that there

is no degradation of the RB5 dye. Therefore, the zeolite was inert to these conditions.

In the case when MNZ uncalcined and with UV radiation were used, the decolouration of RB5 dye occurs. The results show that for concentrations of zeolite of 0.072, 0.170 and 0.510 g/L, the decolouration has similar behavior. However, for concentrations of 0.1 and 1 g/L of MNZ, the behavior is atypical. This change in path of the decolouration is due to heterogeneity of mineral. In this case, due to there are less amount of active sites in the material used. When concentration of the mineral was 1 g/L, initial activity was similar in all cases until 30 minutes, excluding the concentration of 0.1 g/L. Then, decolouration stopped (Figure 11b), it was due to: 1) participation of hydroxyl radicals in unwanted secondary reactions, which blocks removal of dye and decrease the degradation activity [2], or 2) shielding effect of a high concentration of MNZ, which obstructs passage of photons and therefore interaction of radiation with dye molecule, although the active sites increases, it lead to reduction of availability of active sites on the catalyst surface. The effect of UV radiation on zeolite was confirmed, zeolite had a favorable effect, in the treatment of dye at concentrations up to 0.51 g/L. Four curves finished almost at same point when were used 0.072, 0.100, 0.170 and 0.51 g/L of zeolite.

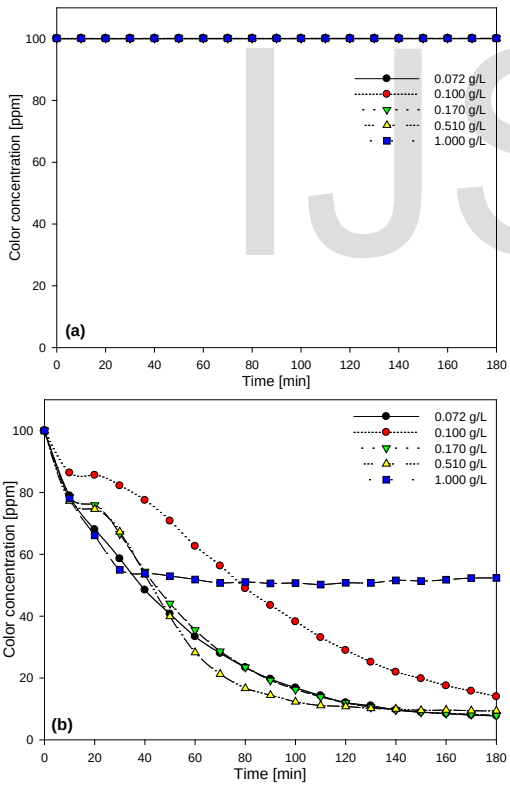


Fig. 11. Decolouration of RB5 using uncalcined MNZ (25 °C): a) without UV radiation, b) with UV radiation.

Furthermore, RB5 dye removal using MNZ calcined at 700 °C without radiation has a similar tendency at three concentrations (0.072, 0.100, 0.170 g/L) and it is observed in Figure 12a. For the same sample at MNZ concentration of 0.51 g/L, a fast decolouration occurs within 40 minutes, after this point, deactivation take place and at the end of the reaction, the color concentration was slightly higher than other MNZ concentrations of (0.072, 0.100, 0.170 g/L). When MNZ concentration of 1 g/L was used, within 100 minutes of reaction it is not observe decolouration, after this point, degradation occurs until a final concentration of 71 ppm. This effect is perhaps due to a shielding effect in the solution, meaning that an increase in the MNZ concentration results in particle agglomeration, following a slight interaction between dye molecule and active sites of material.

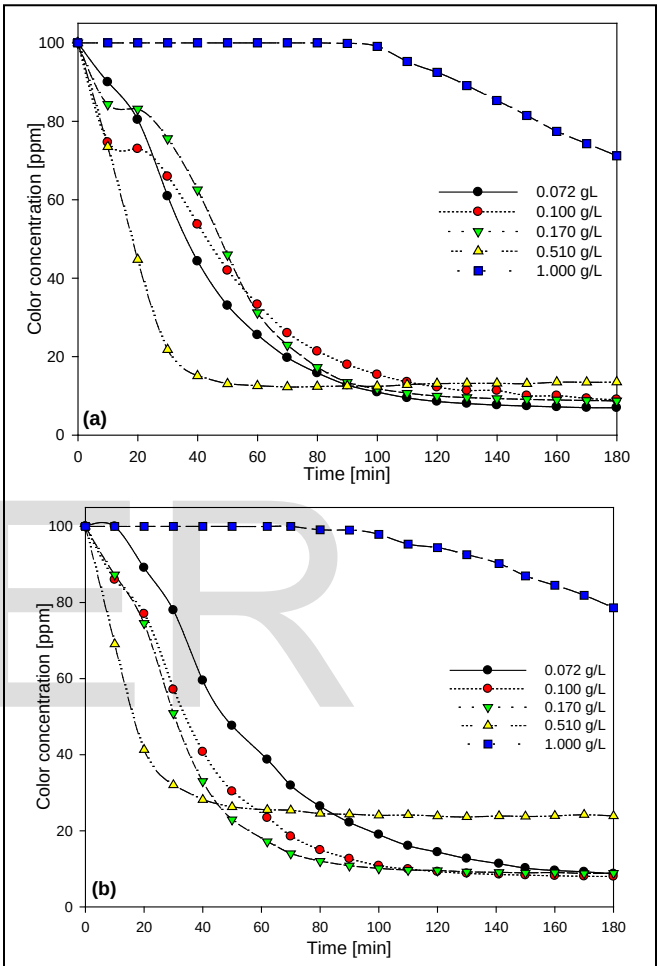


Fig. 12. Decolouration of RB5 using ZNM calcined at 700 °C; a) without UV radiation and b) with UV radiation.

The results of degradation of RB5 dye using MNZ calcined at 700 °C with UV radiation are shown in Figure 12b. For MNZ concentration of 0.072, 0.100 and 0.170 g/L, the tendency of the decolouration is similar but as the concentration of zeolite increases, the rate of decolouration increased, and at the end of reaction the color concentration is the same. While that using 0.51 g/L of MNZ, higher reaction rate was observed up to 20 minutes, meanwhile from 20 to 40 minutes activity was decreased and then zeolite was deactivated at the end of reaction. For MNZ concentration of 0.100, 0.170 g/L, the decolouration process was improved when the UV radiation is employed. Finally, for MNZ concentration of 1 g/L, the decolouration behavior have a similar tendency than the UV radiation is not used. In this case, it was observed that after 180 minutes

of reaction only 22 ppm of chromophore was degraded. This effect is perhaps due to the formation of secondary reactions of decomposition of $H_2O_2$, which do not promote the process of dye degradation. In addition, a possible shielding effect also causes the reaction was carried out slowly. Therefore, there is not good interaction between the dye molecule and the active sites of zeolite, hydroxyl ions and photons.

TOC and IC analysis were performed to determine the degree of mineralization in the degradation process of RB5 dye. Sucrose and sodium carbonate were employed for calibration of TOC and IC, respectively. For all analysis, initial concentrations of dye were kept constant. When uncalcined MNZ and without UV radiation were used (for all concentrations), no change was observed in values of TOC and IC, this effect is due to the lack of activity of MNZ in the degradation process.

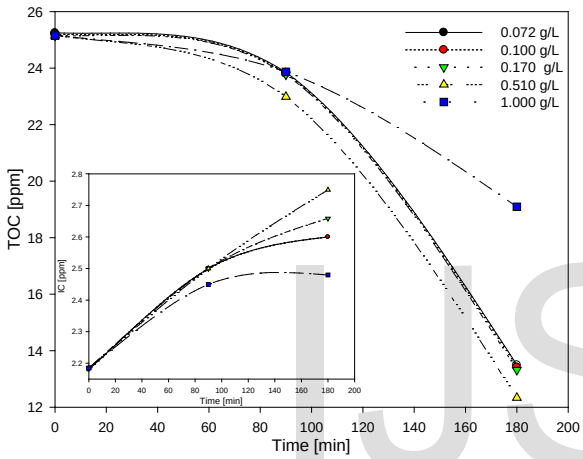


Fig. 13. Variation of TOC and IC in removal of RB5 using uncalcined MNZ (25 °C) with UV radiation.

In Figure 13 the results of TOC and IC for uncalcined MNZ and with UV radiation are shown. Samples were taken at 90 and 180 minutes after starting process of analysis (TOC and IC). At 90 minutes, when concentrations of 0.072, 0.100, 0.170, 1.0 g/L were used, the TOC reduction was 6 % and with concentration of 0.510 g/L was 9 %. At the end of the analysis process (at 180 minutes), it is observed that the concentrations of 0072, 0100 and 0.170 g/L have the same degree of mineralization, however, for concentration of 0.51 g/L, the degree of mineralization is slightly greater than in the other concentrations. For the concentration of 1 g/L, the degree of mineralization is less than the other concentrations. These results are agreed with those obtained in the decolouration process. In addition, IC measures showed that for MNZ concentrations of 0.072, 0.100, 0.170 and 0.510 g/L and at 90 minutes, the IC values were practically the same, but when MNZ concentration of 1 g/L was used, the concentration of IC was lowest. At 180 minutes of reaction, the amount of inorganic matter increase for all cases is proportional to the MNZ concentration, with exception of MNZ concentration of 1 g/L.

In Figure 14a, the results of TOC and IC analysis for degradation reactions of RB5 dye, using MNZ calcined at 700 ° C and without UV radiation, are shown. It is observed at 90 minutes, the behavior is similar to that shown in the previous Figure. For MNZ concentration of 0.51 g/L, a further reduction in organic matter was observed that when using the other MNZ concentrations. However, at 180 minutes of reaction, the organic matter was similar for all cases without zeolite concentration of 1 g/L. The same effect is observed in the IC determination, mainly due that at the end of reaction the activity decreases.

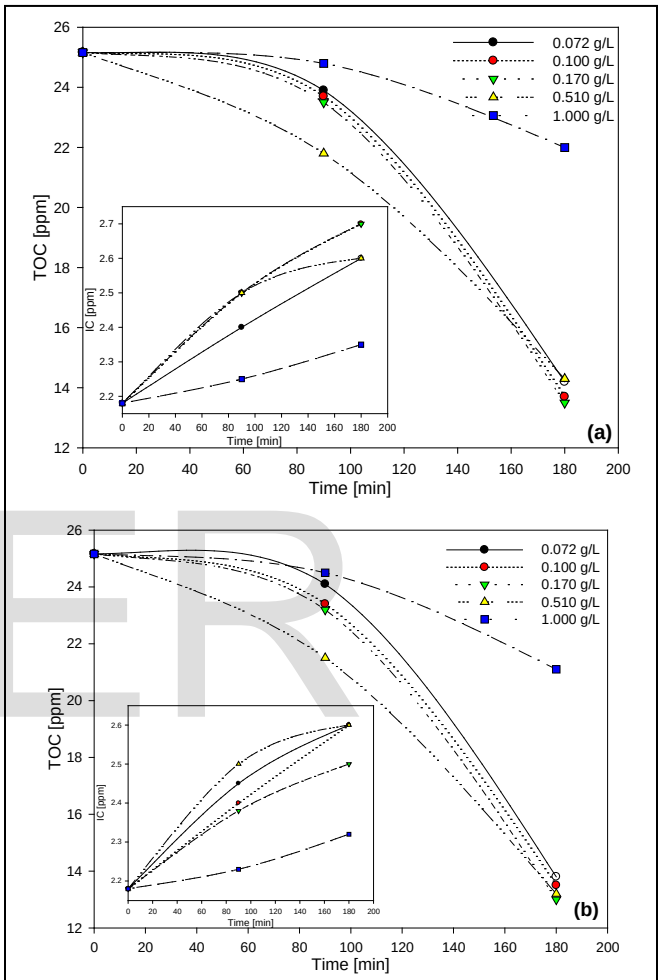


Fig. 14. Decolouration of RB5 using ZNM calcined at 700 °C; a) without UV radiation and b) with UV radiation.

Finally, the removal of TOC for MNZ calcined at 700 °C and with UV radiation is shown in Figure 14b. At 90 minutes, the TOC concentrations have a slightly higher dispersion respect to the previously case discussed. As in the previous case, the concentration of zeolite of 0.51 g/L showed the highest removal of TOC. However at 180 minutes, for all zeolite concentrations, lower that 1 g/L, show the same trend. For MNZ concentration of 1 g/L, it is observed that the formation of IC was small. Otherwise, for the other MNZ concentrations, the results of IC not show a trend respect the concentration of zeolite.

## 4. Conclusions

In this work, the characterization of Mexican Natural Zeolite

was performed using different techniques, and it was found mainly clinoptilolite (XRD), containing approximately 2.6 % of $Fe_2O_3$ (by AA technique) and traces of $TiO_2$ (by AA technique). The calcination of MNZ from 200 °C to 700 °C has not impact in the global material composition. It was also found that the zeolite is a mesoporous material and its surface area decreases when the calcination temperature increases.

The material has been activated at 25 °C of temperature using a UV radiation since there is no activity without it.

The catalytic activity of material was improved when increase the calcined temperature during the decolouration process. However, at the end of reaction and for the cases where the zeolitic material is activated (at low concentrations), a similar degree of decolouration is reached.

The best removal of color was 85 % at low concentrations of MNZ and the Total Organic Carbon decreases in the range of (50 – 60) %.

## Acknowledgements

The authors would like to thank the Instituto Politécnico Nacional and CONACyT for the financial support, Extractive Metallurgical Laboratory-ESIQIE and the Centro de Nanociencias y Micro y Nanotecnologías-IPN for facilities to obtain the characterization of MNZ.

## References

[1] P. Bosch, I. Schifter, "La zeolita una piedra que hierve", Fondo de cultura economica, Mexico, 1997.
[2] S. Navalon, M. Alvaro, and H. Garcia, "Heterogeneous Fenton catalysts based on clays, silicas and zeolites," *Appl. Catal. B Environ.*, vol. 99, no. 1–2, pp. 1–26, 2010.
[3] T. Gebremedhin-Haile, M. T. Olguín, and M. Solache-Ríos, "Removal of mercury ions from mixed aqueous metal solutions by natural and modified zeolitic minerals", *Water. Air. Soil Pollut.*, vol. 148, pp. 179–200, 2003.
[4] D. W. Breck, "Zeolite Molecular Sieves", John Wiley & Sons, Inc., New York, 1974.
[5] S Wang, Y Peng, "Natural zeolites as effective adsorbents in water and wastewater treatment", *Chem. Eng. J.*, vol. 156, no. 1, pp. 11-24, 2010.
[6] A. H. Englert and J. Rubio, "Characterization and environmental application of a Chilean natural zeolite", *Int. J. Miner. Process.*, vol. 75, pp. 21–29, 2005.
[7] S. M. Auerbach, K. A. Carrado, P. K. Dutta, "Handbook of Zeolites Science and Technology", Marcel Dekker, Inc., New York, 2003.
[8] T. F. Degnan, "Applications of zeolites in petroleum refining", *Top. Catal.*, vol. 13, pp. 349–356, 2000.
[9] C. de las Pozas, D. Díaz Quintanilla, J. Pérez-Pariente, R. Roque-Malherbe, and M. Magi, "Hydrothermal transformation of natural clinoptilolite to zeolites Y and P1: Influence of the Na, K content", *Zeolites*, vol. 9, pp. 33–39, 1989.
[10] M. R. Eskandarian, M. Fazli, M. H. Rasoulifard, and H. Choi, "Decomposition of organic chemicals by zeolite-TiO2 nanocomposite supported onto low density polyethylene film under UV-LED powered by solar radiation", *Appl. Catal. B Environ.*, vol. 183, pp. 407–416, 2016.
[11] J. P. Bellat, I. Bezverkhyy, G. Weber, S. Royer, R. Averlant, J. M. Giraudon, and J. F. Lamonier, "Capture of formaldehyde by adsorption on nanoporous materials", *J. Hazard. Mater.*, vol. 300, pp. 711–717, 2015.
[12] G. Sanchez, B. Z. Dlugogorski, E. M. Kennedy, and M. Stockenhuber, "Zeolite-supported iron catalysts for allyl alcohol synthesis from glycerol", *Appl. Catal. A Gen.*, vol. 509, pp. 130–142, 2016.
[13] Y. P. Wei, D. Q. Wei, and H. W. Gao, "Treatment of dye wastewater by in situ hybridization with Mg-Al layered double hydroxides and reuse of dye sludge", *Chem.Eeng. J.*, vol. 172, pp. 872–878, 2011.
[14] F. P. Van Der Zee, "Anaerobic azo dye reduction", Thesis, Netherlands, 2002.
[15] C. C. I. Guaratini and M. V. B. Zanoni, "Corantes têxteis", *Quimica Nova*, vol. 23, pp. 71–78, 2000.
[16] T. H. Kim, C. Park, E. B. Shin, and S. Kim, "Decolorization of disperse and reactive dye solutions using ferric chloride", *Desalination*, vol. 161, pp. 49–58, 2004.
[17] Y. Al-Degs, M. a M. Khraisheh, S. J. Allen, M. N. Ahmad, and G. M. Walker, "Competitive adsorption of reactive dyes from solution: Equilibrium isotherm studies in single and multisolute systems", *Chem. Eng. J.*, vol. 128, pp. 163–167, 2007.
[18] A. W. M. Ip, J. P. Barford, and G. McKay, "A comparative study on the kinetics and mechanisms of removal of Reactive Black 5 by adsorption onto activated carbons and bone char", *Chem. Eng. J.*, vol. 157, pp. 434–442, 2010.
[19] A. L. Ahmad, and S. W. Puasa, "Reactive dyes decolourization from an aqueous solution by combined coagulation/micellar-enhanced ultrafiltration process", *Chem. Eng. J.*, vol. 132, pp. 257–265, 2007.
[20] S. M. Ghoreishi and R. Haghighi, "Chemical catalytic reaction and biological oxidation for treatment of non-biodegradable textile effluent", *Chem. Eng. J.*, vol. 95, pp. 163–169, 2003.
[21] R. S. Shertate and P. Thorat, "Biotransformation of Textile Dyes: a Bioremedial Aspect of Marine Environment", *Am. J. Environ. Sci.*, vol. 10, pp. 489–499, 2014.
[22] K. Guesh, M. J. López-Muñoz, C. Márquez-Álvarez, Y. Chebude, I. Diaz, "Ethiopian natural zeolites for photocatalysis", *Bull. Chem. Soc. Ethiop.*, vol. 29, no. 3, pp. 431-440, 2015.
[23] S. Brunauer, P. H. Emmett, and E. Teller, "Adsorption of Gases in Multimolecular Layers", *J. Am. Chem. Soc.*, vol. 60, pp. 309–319, 1938.
[24] J. H. de Boer, B. C. Lippens, B. G. Linsen, J. C. P. Broekhoff, A. van den Heuvel, and Th. J. Osinga, "Thet-curve of multimolecular $N_2$-adsorption", *J. Colloid Interf. Sci.*, vol. 21, pp. 405–414, 1966.
[25] F. N. Gu, F. Wei, J. Y. Yang, N. Lin, W. G. Lin, Y. Wang, and J. H. Zhu, "New strategy to synthesis of hierarchical mesoporous zeolites", *Chem. Mater.*, vol. 22, pp. 2442–2450, 2010.
[26] J. C. Groen and J. Perez-Ramirez, "Critical appraisal of mesopore characterization by adsorption analysis", *Appl.*

*Catal. A Gen.*, vol. 268, pp. 121–125, 2004.
[27] R. Wise, W., Tschernich, "The chemical compositions and origin of the zeolites offretite, erionite, and levyne", *Am. Mineral.*, vol. 61, pp. 853–863, 1976.
[28] M. Pamba, G. Maurin, S. Devautour, J. Vanderschueren, J. C. Giuntini, F. Di, F. Hamidi, Ï. E. Normale, M. Cedex, D. Chimie, and U. Ï. Oran, "Influence of framework Si / Al ratio on the Na+/ mordenite interaction energy", *Pccp*, vol. 2, pp. 2027–2031, 2000.
[29] V. N. Smirenskaya, and V. I. Vereshchagin, "Prospects of using zeolite rocksof Siberian in silicate materials", *Glass and Ceramics*, vol. 59, pp. 414–419, 2002.
[30] D. L. Bish, and D. W. Ming, "Natural Zeolites: Occurrence, Properties, Applications", *Mineralogical Society of America*, vol. 45. pp. 654, 2001
[31] P. Ballirano, and G. Cametti, "Dehydration dynamics and thermal stability of erionite-K: Experimental evidence of the "internal ionicexchange" mechanism", *Micropor. Mesopor. Mat.*, vol. 163, pp. 160–168, 2012.
[32] A. Alberti, "The Crystal Structure of Two Clinoptilolites", *Tschermaks Min. Petr. Mitt.*, vol. 22, pp. 25–37, 1975.
[33] H. Sasaki, Y. Oumi, K. Itabashi, B. Lu, T. Teranishi, and T. Sano, "Direct hydrothermal synthesis and stabilization of high-silica mordenite (Si:Al = 25) using tetraethylammonium and fluoride ions", *J. Mater. Chem.*, vol. 13, pp. 1173–1179, 2003.
[34] X. Liu, G. Chen, J. G. Erwin, and C. Su, "Silicon impurity release and surface transformation of TiO2 anatase and rutile nanoparticles in water environments", *Environ. Pollut.*, vol. 184, pp. 570-578, 2014.
[35] J. H. Bang, and K. S. Suslick, "Sonochemical Synthesis of Nanosized Hollow Hematite", *J. Am. Chem. Soc.*, vol. 129, pp. 2242–2243, 2007.
[36] M. C. Huang, W. S. Chang, J. C. Lin, Y. H. Chang, and C. C. Wu, "Magnetron sputtering process of carbon-doped α-Fe2O3 thin films for photoelectrochemical water splitting", *J. Alloy Compd.*, vol. 636, pp. 176–182, 2015.
[37] W. Mozgawa, "The relation between structure and vibrational spectra of natural zeolites", *J. Mol. Struct.*, vol. 596, pp.129-137, 2001.
[38] L. V. Gasparov, D. Arenas, K.-Y. Choi, G. Güntherodt, H. Berger, L. Forro, G. Margaritondo, V. V. Struzhkin, and R. Hemley, "Magnetite: Raman study of the high-pressure and low-temperature effects", *J. Appl. Phys.*, vol. 97, pp. 10A922, 2005.
[39] L. Slavov, M. V. Abrashev, T. Merodisska, Ch. Gelev, R. E. Vandenberghe, I. Markova-Deneva, and I. Nedkov, "Raman spectroscopy investigation of magnetite nanoparticles in ferrofluids", *J. Magn. Magn. Mater.*, vol. 322, pp. 1904-1911, 2010.
[40] Y. Li, Z. Feng, H. Xin, F. Fan, J. Zhang, P. C. M. M. Magusin, E. J. M. Hensen, R. A. Van Santen, Q. Yang, and C. Li, "Effect of aluminum on the nature of the iron species in Fe-SBA-15", *J. Phys. Chem. B*, vol. 110, pp. 26114–26121, 2006.
[41] F. Chávez-Rivas, G. Rodríguez-Fuentes, G. Berlier, I. Rodríguez-Iznaga, V. Petranovskii, R. Zamorano-Ulloa, and S. Coluccia, "Evidence for controlled insertion of Fe ions in the framework of clinoptilolite natural zeolites", *Microporous Mesoporous Mater.*, vol. 167, pp. 76–81, 2013.
[42] M. S. Kumar, M. Schwidder, W. Grünert, and A. Brückner, "On the mature of different iron sites and their catalytic role in Fe-ZSM-5 DeNOx catalysts: new insights by a combined EPR and UV/VIS spectroscopic approach", *J. Catal.*, vol. 227, pp. 384-397, 2004.
[43] S. Bordiga, R. Buzzoni, F. Geobaldo, C. Lamberti, E. Giamello, A. Zecchina, G. Leofanti, G. Petrini, G. Tozzola, and G. Vlaic, "Structure and reactivity of framework and estraframework iron in Fe-silicate as investigated by spectroscopic and physicochemical methods", *J. Catal.*, vol. 158, pp. 486–501, 1996.
[44] K. S. W. Sing, "Reporting physisorption data for gas/solid systems with special reference to the determination of surface area and porosity", *Pure Appl. Chem.*, vol. 57, pp. 603–619, 1985.
[45] S. J. Gregg, and K. S. W. Sing, "Adsorption, Surface Area and Porosity", Academic Press, London, 1982.